Excitation of spin-isospin modes in the quasifree scattering region

M. Ichimura and K. Kawahigashi
Institute of Physics, College of Arts and Science, University of Tokyo, Komaba, Tokyo 153, Japan

T. S. Jørgensen and C. Gaarde
Niels Bohr Institute, University of Copenhagen, DK-2100 Copenhagen, Denmark
(Received 16 December 1988)

Nuclear spin longitudinal and transverse response functions in the isovector channel are calculated by the continuum random-phase approximation with the orthogonality condition. This method treats the nucleus as of finite size and with a continuum single-particle spectrum. It can include an imaginary potential for the particle states. The corresponding longitudinal and transverse cross sections for ^{40}Ca(p,p') at $E_p=500$ MeV are calculated by distorted-wave impulse approximation fully quantum mechanically which is beyond the previous analyses by the Glauber approximation. The results are compared with the longitudinal-transverse response ratio extracted from the polarization transfer observables of the Los Alamos experiment. Large effects of the finiteness of the nucleus are seen especially in the longitudinal response. Effects of the distortion diminish the softening and hardening due to nuclear correlation, but the enhancement and quenching still remain. These effects cooperatively reduce the ratio.

I. INTRODUCTION

The investigation of the nuclear response to external spin-isospin fields is one of the central issues in current nuclear physics. Depending on the transferred energy ω and momentum q to the nucleus, different physics can be studied, such as giant Gamov-Teller resonances in the low-q and low-ω region, delta-hole excitation for larger ω, etc.

The study of the quasifree scattering region with medium momentum transfer ($q\approx 1.5$–2.5 fm^{-1}) is a newly developed field. If the incident particle interacts freely with a nucleon in the nucleus and the motion of the nucleon can be regarded simply as the Fermi motion, one expects a broad bump in the energy spectrum with a peak at $\omega=q^2/2m$ (m being the nucleon mass) and a width determined by the Fermi momentum. We call it the quasifree bump. Experiments clearly show the bump but occasionally the peak energy deviates from the simple expectation.

Alberico *et al.*[1] pointed out an interesting contrast between the isovector spin longitudinal and transverse modes produced by the operators

$$O_L(\mathbf{q})=i\sum_{i=1}^{A}\tau^i(\boldsymbol{\sigma}^i\cdot\mathbf{q})e^{i\mathbf{q}\cdot\mathbf{r}_i}/\sqrt{2}\ , \tag{1.1}$$

$$O_T(\mathbf{q})=i\sum_{i=1}^{A}\tau^i(\boldsymbol{\sigma}^i\times\mathbf{q})e^{i\mathbf{q}\cdot\mathbf{r}_i}/2\ , \tag{1.2}$$

respectively, where $\boldsymbol{\sigma}^i$, $\boldsymbol{\tau}^i$, and $\mathbf{r}_i$ are the spin, the isospin, and the coordinate vector of the ith nucleon. The prediction was based on the random-phase approximation (RPA) calculation in nuclear matter with one-pion exchange (OPE) plus one-rho-meson exchange plus a contact interaction specified by the Landau-Migdal parameter g' ($\pi+\rho+g'$ model). The prediction was that around $q=1.75$ fm^{-1} (the critical momentum for pion condensation), the response function for the isovector spin longitudinal mode, $R_L(q,\omega)$ is enhanced and softened due to OPE attraction,[2] while that for the isovector spin transverse mode, $R_T(q,\omega)$, is quenched and hardened due to the short-range correlation.[1] The feature can be seen in the Fermi gas results of Fig. 4.

Some experimental results are summarized[3–5] in Fig. 1, where the positions of the quasifree peaks seen in the reactions (e,e'),[6] (p,p'),[7] and $(^3\mathrm{He},t)$ (Ref. 3) are compared with the line $\omega=q^2/2m$ in the q-ω plane. The peak observed in $(d,2p)$ (Refs. 4 and 8) falls on the same line as $(^3\mathrm{He},t)$. One of the eminent features seen in the figure is gradual softening of $(^3\mathrm{He},t)$ with respect to (e,e') as q increases. This feature might be explained in the following way.[3–5] First (e,e') does not excite the spin longitudinal modes. Second, spin-dependent forces dominate for charge exchange reactions at intermediate energy. Third, for $q>0.8$ fm^{-1}, the spin longitudinal part of the forces is getting relatively stronger than the spin transverse one, as q becomes larger (see Fig. 2). Therefore, the softening of $R_L(q,\omega)$ does not affect (e,e') but might have larger effects on the spectrum of $(^3\mathrm{He},t)$ as q increases. Numerical analysis of Alberico *et al.*[5] supports this expectation.

Efforts to isolate the spin longitudinal and transverse response functions are carried out by elaborate measurements of spin observables. The ratio "R_L/R_T" is estimated by the plane-wave impulse approximation (PWIA) analysis from the complete polarization transfer measurement of (p,p') at 500 MeV performed at Clinton P. Anderson Meson Physics Facility (LAMPF) (Refs. 9 and 10) for various ω at $q=1.75$ fm^{-1}. The obtained ratio is close to unity, which completely contradicts the prediction.[1] Preliminary results of the measurement of

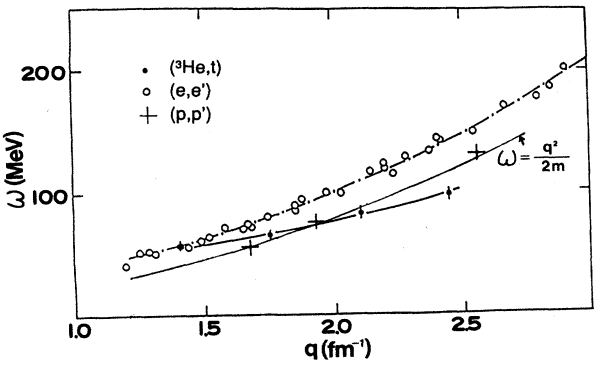

FIG. 1. The quasifree peak positions seen in (e,e') (dash-dotted line with open circles), (p,p') (+), and $(^3\mathrm{He},t)$ (solid line with solid circles) are compared with the $\omega=q^2/2m$ line in the q-ω plane.

the tensor analyzing power of $^{40}\mathrm{Ca}(\vec{d},2p)$ (Ref. 8) also support the results of LAMPF. The discrepancy is, at the moment, considered[5,10–21] to be ascribed to the distortion (mainly absorption) of the probes, the finiteness of the nucleus, and a larger g' than used in Ref. 1.

Effects of the finiteness appear through the density dependence of the collectivity and the mixing of the spin longitudinal and transverse modes. They have been taken into account by various means. The simplest one may be the Fermi gas model with a local density approximation (LDA).[12,13] The semiclassical approach,[22] a sophisticated version of LDA, is applied to the present problem.[14] The method is elaborated by including $O(\hbar^2)$ contributions.[17] The semi-infinite slab (SIS) model developed by Esbensen and Bertsch[23] has also been applied by Esbensen *et al.*[10,12] Another approach is the bound-state approximation in solving RPA in which single-particle states are represented by bound states truncated in a certain space.[5,14,16] The bound states in a harmonic oscillator potential are often used. Alberico *et al.*[5,14,15] further employed an additional approximation of Toki and Weise.[25] Shigehara *et al.*[18,19] have utilized the continuum RPA method of Shlomo and Bertsch[24] which fully takes into account the continuum nature of the particle states and hence the escape width. So far this is the most advanced analysis of the finiteness. However, this technique is not applicable if the particles and holes are in different potentials, e.g., the holes are in the bound state of the real potential but the particles move in the complex optical potential.[26] In this paper we adopt the continuum RPA with the orthogonality condition (hereafter called OCRPA) developed by Izumoto,[27] which allows the particles and holes to be in different potentials.

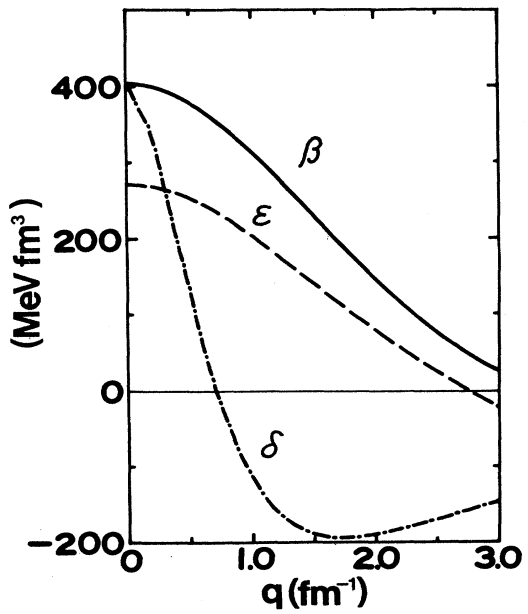

FIG. 2. The q dependence of the real parts of the NN t-matrix amplitudes β, δ, and ϵ at $E_p=515$ MeV.

Up to now the effects of the distortion have been treated poorly. In most analyses of SIS (Refs. 12 and 10) and LDA,[13,16] the effects of the absorption have only been taken into account in terms of a Glauber approximation with straight line trajectories. The distortion of the trajectory and the spin reorientation during scattering are rarely included.[21] A surface response approximation in the angular momentum representation used by Refs. 5, 14, 17, and 18 treats the distortion in a cruder way. Namely, in the Glauber approximation the damping effect of the absorption is expressed by a function of the impact parameter b, $F(b)$. However, in the surface response approximation the damping function $F(b)$ is simply replaced by the same function of the radius r, $F(r)$. This geometrical difference between cylindrical and spherical shape could be serious. In ordinary Glauber approximations such as SIS,[12] the softening and the hardening are reduced by the absorption, but not so in the surface approximation.[14,18] This may be due to the wrong geometry of the latter.

There have been a few full quantum-mechanical calculations including the distortion.[28,29] In this paper we present results of a calculation in a distorted-wave impulse approximation (DWIA). Significant effects of the distortion are observed in such an approximation.

In Sec. II we give the formalism for calculating the response functions by means of OCRPA, and the DWIA formalism in terms of the response function in r space. In Sec. III the energy spectra of the response functions, R_L and R_T, for ^{40}Ca are shown for various q. Effects of the finiteness of the nucleus are clearly seen. The smearing of the narrow structures at low energies due to the absence of the spreading width is done by using a complex optical potential for the particle states. A bound-state approximation is tested. In Sec. IV, we present the energy spectra of the DWIA cross sections for $^{40}\mathrm{Ca}(p,p')$ at $E_p=500$ MeV. The dependence on the transferred multipolarity is investigated and the contribution from each hole state is studied. The ratios R_L/R_T obtained by the LAMPF experiment are compared with our results in Sec. V. The combined effects of the finiteness and the dis-

tortion are found to reduce the ratio drastically. Future problems are discussed in Sec. VI and a summary is given in Sec. VII.

II. FORMALISM

In this section we present the formalism of the continuum RPA with the orthogonality condition (OCRPA) and apply it to the DWIA calculation of the double differential cross section $d^2\sigma/d\Omega\, d\omega$ for nucleon-nucleus inelastic scattering to the continuum states. In Sec. II A we explain the significance of the orthogonality condition and show how to incorporate the condition with the continuum RPA based on Ref. 27. We then introduce the spin-isospin polarization propagators and show how to calculate them in the framework of OCRPA. Then we derive, following Ref. 30, the formula for the spin-isospin response functions obtained from the corresponding polarization propagators.

In Sec. II B we first give the t matrix of the free NN scattering and discuss the problem of nonlocality. Then we present the detailed formulas for the DWIA cross sections based on Ref. 28. The formulas for the response functions and cross sections are given in angular momentum representation which is convenient for the finite nucleus case.

A. Polarization propagators and response functions and the orthogonality condition

1. Two-point particle-hole Green's function

To explain the method of OCRPA in a simple way, we omit the spin and isospin suffices. First, we define the two-point particle-hole Green's function as follows:

$$\Pi(\mathbf{r},\mathbf{r}';\omega)=\langle 0|\hat{\psi}^\dagger(\mathbf{r})\hat{\psi}(\mathbf{r})\frac{1}{\hbar\omega-(H-E_0)+i\eta}\hat{\psi}^\dagger(\mathbf{r}')\hat{\psi}(\mathbf{r}')+\hat{\psi}^\dagger(\mathbf{r}')\hat{\psi}(\mathbf{r}')\frac{1}{-\hbar\omega-(H-E_0)+i\eta}\hat{\psi}^\dagger(\mathbf{r})\hat{\psi}(\mathbf{r})|0\rangle\ , \tag{2.1}$$

where $H=H_{\rm sp}+V$ is the total Hamiltonian of the nucleus and $|0\rangle$ and E_0 are the ground state and its energy, respectively. $H_{\rm sp}$ is the single-particle Hamiltonian which represents the mean field and V is the residual interaction. $\hat{\psi}(\mathbf{r})$ is the nucleon annihilation operator at the point $\mathbf{r}$, which can be expressed as

$$\hat{\psi}(\mathbf{r})=\sum_\alpha \phi_\alpha(\mathbf{r})\hat{a}_\alpha\ , \tag{2.2}$$

where $\hat{a}_\alpha$ is the annihilation operator for the state α, whose wave function $\phi_\alpha(\mathbf{r})$ satisfies the equation

$$H_{\rm sp}\phi_\alpha=\epsilon_\alpha\phi_\alpha\ . \tag{2.3}$$

To calculate Π of (2.1) by means of RPA, one must prepare the free (uncorrelated) Green's function Π^0 defined as

$$\Pi^0(\mathbf{r},\mathbf{r}';\omega)\equiv\sum_{ph}\left[\frac{\phi_h^\dagger(\mathbf{r})\phi_p(\mathbf{r})\phi_p^\dagger(\mathbf{r}')\phi_h(\mathbf{r}')}{\hbar\omega-(\epsilon_p-\epsilon_h)+i\eta}+\frac{\phi_h^\dagger(\mathbf{r}')\phi_p(\mathbf{r}')\phi_p^\dagger(\mathbf{r})\phi_h(\mathbf{r})}{-\hbar\omega-(\epsilon_p-\epsilon_h)+i\eta}\right]\ , \tag{2.4}$$

where p and h denote the particle and the hole state, respectively. Then, a problem is how to treat the sum over the continuum states,

$$g^p(\mathbf{r},\mathbf{r}';E)\equiv\sum_p\frac{\phi_p(\mathbf{r})\phi_p^\dagger(\mathbf{r}')}{E-\epsilon_p+i\eta}\ . \tag{2.5}$$

Shlomo and Bertsch[24] pointed out that one can replace the sum over p by that over the complete set α, and wrote Π^0 as

$$\Pi^0(\mathbf{r},\mathbf{r}';\omega)=\sum_h[\phi_h^\dagger(\mathbf{r})g(\mathbf{r},\mathbf{r}';\hbar\omega+\epsilon_h)\phi_h(\mathbf{r}')+\phi_h^\dagger(\mathbf{r}')g(\mathbf{r}',\mathbf{r};-\hbar\omega+\epsilon_h)\phi_h(\mathbf{r})]\ , \tag{2.6}$$

with the single-particle Green's function

$$g(\mathbf{r},\mathbf{r}';E)\equiv\langle\mathbf{r}|\frac{1}{E-H_{\rm sp}+i\eta}|\mathbf{r}'\rangle=\sum_\alpha\frac{\phi_\alpha(\mathbf{r})\phi_\alpha^\dagger(\mathbf{r}')}{E-\epsilon_\alpha+i\eta}\ . \tag{2.7}$$

The sum over α is not equivalent to that over p, i.e.,

$$\sum_{\alpha h}\left[\frac{\phi_h^\dagger(\mathbf{r})\phi_\alpha(\mathbf{r})\phi_\alpha^\dagger(\mathbf{r}')\phi_h(\mathbf{r}')}{\hbar\omega-(\epsilon_\alpha-\epsilon_h)+i\eta}+\frac{\phi_h^\dagger(\mathbf{r}')\phi_\alpha(\mathbf{r}')\phi_\alpha^\dagger(\mathbf{r})\phi_h(\mathbf{r})}{-\hbar\omega-(\epsilon_\alpha-\epsilon_h)+i\eta}\right]$$
$$=\sum_{ph}\left[\frac{\phi_h^\dagger(\mathbf{r})\phi_p(\mathbf{r})\phi_p^\dagger(\mathbf{r}')\phi_h(\mathbf{r}')}{\hbar\omega-(\epsilon_p-\epsilon_h)+i\eta}+\frac{\phi_h^\dagger(\mathbf{r}')\phi_p(\mathbf{r}')\phi_p^\dagger(\mathbf{r})\phi_h(\mathbf{r})}{-\hbar\omega-(\epsilon_p-\epsilon_h)+i\eta}\right]$$
$$+\sum_{h'h}\left[\frac{\phi_h^\dagger(\mathbf{r})\phi_{h'}(\mathbf{r})\phi_{h'}^\dagger(\mathbf{r}')\phi_h(\mathbf{r}')}{\hbar\omega-(\epsilon_{h'}-\epsilon_h)+i\eta}+\frac{\phi_h^\dagger(\mathbf{r}')\phi_{h'}(\mathbf{r}')\phi_{h'}^\dagger(\mathbf{r})\phi_h(\mathbf{r})}{-\hbar\omega-(\epsilon_{h'}-\epsilon_h)+i\eta}\right]\ . \tag{2.8}$$

Since the second term of the right-hand side vanishes except for $\omega=\epsilon_{h'}-\epsilon_h$, there is no practical problem in Shlomo-Bertsch's method. However, if one uses a different $H_{\rm sp}$ for g from that for the occupied states ϕ_h (e.g., in case of including an imaginary potential to $H_{\rm sp}$ for g as is mentioned in Sec. I), this cancellation does not occur any more and one cannot use this method. Noting that the particle states must be orthogonal to the occupied states, we assume that g^p is expressed by the single-particle Green's function in the orthogonality condition model, $g^{\rm oc}$, introduced by Izumoto and Mori,[31] which satisfies the condition

$$\Lambda(E-H_{\rm sp}+i\eta)\Lambda g^{\rm oc}=\Lambda\ , \qquad \Gamma g^{\rm oc}=0\ , \tag{2.9}$$

with

$$\Lambda=\sum_p|\phi_p(\mathbf{r})\rangle\langle\phi_p(\mathbf{r}')|\ , \qquad \Gamma=1-\Lambda=\sum_h|\phi_h(\mathbf{r})\rangle\langle\phi_h(\mathbf{r}')|\ . \tag{2.10}$$

The solution is written as

$$g^{\rm oc}=g-g\Gamma(\Gamma g\Gamma)^{-1}\Gamma g\ . \tag{2.11}$$

Hence, we can rewrite Π^0 as

$$\Pi^0(\mathbf{r},\mathbf{r}';\omega)=\sum_h[\phi_h^\dagger(\mathbf{r})g^{\rm oc}(\mathbf{r},\mathbf{r}';\hbar\omega+\epsilon_h)\phi_h(\mathbf{r}') +\phi_h^\dagger(\mathbf{r}')g^{\rm oc}(\mathbf{r}',\mathbf{r};-\hbar\omega+\epsilon_h)\phi_h(\mathbf{r})]\ . \tag{2.12}$$

The Green's functions, g and $g^{\rm oc}$, are expressed as

$$g(\mathbf{r},\mathbf{r}';E)=\sum_{ljm}\mathcal{Y}^\dagger_{ljm}(\hat{\mathbf{r}})\frac{g_{lj}(r,r';E)}{rr'}\mathcal{Y}_{ljm}(\hat{\mathbf{r}}')\ , \tag{2.13}$$

where

$$\mathcal{Y}_{ljm}(\hat{\mathbf{r}})=\sum_{m_l}\langle lm_l\tfrac{1}{2}m_s|jm\rangle i^l Y_{lm_l}(\hat{\mathbf{r}})|\chi_{(1/2)m_s}\rangle\ . \tag{2.14}$$

The radial part g_{lj} is

$$g_{lj}(r,r';E)=\sum_\epsilon f_{lj}(r,\epsilon)\frac{1}{E-\epsilon+i\eta}f^*_{lj}(r',\epsilon) =\frac{2\tilde{\mu}}{\hbar^2}f_{lj}(r_<,E)h_{lj}(r_>,E)/W(f_{lj},h_{lj})\ , \tag{2.15}$$

where $f_{lj}(r,\epsilon)$ and $h_{lj}(r,\epsilon)$ are the regular and the irregular solution of $H_{\rm sp}$ with the energy ϵ, respectively, and $r_{<(>)}$ denotes the smaller(larger) one of r and r'. The denominator W denotes the Wronskian, and $\tilde{\mu}$ $[=(A-1)m/A]$ is the reduced mass between the particle and the rest nucleus. From (2.11) and (2.15), the radial part of $g^{\rm oc}$ is given by

$$g^{\rm oc}_{lj}(r,r';E)=g_{lj}(r,r';E) -\sum_{n_h n_h'}\int_0^\infty dr_1\int_0^\infty dr_2\left\{g_{lj}(r,r_1;E)u_{n_h lj}(r_1)\left[\int_0^\infty dr_3\int_0^\infty dr_4 u_{n_h'' lj}(r_3)g_{lj}(r_3,r_4;E)u_{n_h''' lj}(r_4)\right]^{-1}_{n_h n_h'} \times u_{n_h' lj}(r_2)g_{lj}(r_2,r';E)\right\}\ , \tag{2.16}$$

where $u_{n_h lj}(r)$ is the radial part of the occupied-state wave function with the node n_h and $[\ ]^{-1}_{n_h n_h'}$ denotes the n_h,n_h' component of the inversed matrix $[\ ]^{-1}$.

2. *Spin-isospin polarization propagator*

We define the spin-isospin current $\hat{j}_{\mu a}(\mathbf{r})$ as

$$\hat{j}_{\mu a}(\mathbf{r})\equiv i\sum_{i=1}^A\tau_a^i\sigma_\mu^i\delta(\mathbf{r}-\mathbf{r}_i)=i\sum_{lJM}\langle lm\,1\mu|JM\rangle\hat{j}^\dagger_{lJMa}(r)i^l Y_{lm}(\hat{\mathbf{r}})\ , \tag{2.17}$$

where $\mu=0,\pm1$ and $a=x,y,z$. The radial part is given by

$$\hat{j}_{lJMa}(r)=\sum_{i=1}^A\tau_a^i\frac{\delta(r-r_i)}{rr_i}[i^l Y_l(\hat{\mathbf{r}}_i)\times\sigma^i]^J_M\ . \tag{2.18}$$

The polarization propagator for the spin-isospin current is written, in the $\vec{r}$ representation, as

$$\begin{aligned}\Pi_{\mu a\nu b}(\mathbf{r},\mathbf{r}';\omega)&\equiv\sum_n\left[\frac{\langle0|\hat{j}_{\mu a}(\mathbf{r})|n\rangle\langle n|\hat{j}^\dagger_{\nu b}(\mathbf{r}')|0\rangle}{\hbar\omega-(E_n-E_0)+i\eta}+\frac{\langle0|\hat{j}^\dagger_{\nu b}(\mathbf{r}')|n\rangle\langle n|\hat{j}_{\mu a}(\mathbf{r})|0\rangle}{-\hbar\omega-(E_n-E_0)+i\eta}\right]\\ &=\langle0|\left[\hat{j}_{\mu a}(\mathbf{r})\frac{1}{\hbar\omega-(H-E_0)+i\eta}\hat{j}^\dagger_{\nu b}(\mathbf{r}')+\hat{j}^\dagger_{\nu b}(\mathbf{r}')\frac{1}{-\hbar\omega-(H-E_0)+i\eta}\hat{j}_{\mu a}(\mathbf{r})\right]|0\rangle\\ &=\delta_{ab}\sum_{JM}\sum_{l_1m_1}\sum_{l_2m_2}\Pi_{Jl_1l_2a}(r,r';\omega)\langle l_1m_1\,1\mu|JM\rangle\langle l_2m_2\,1\nu|JM\rangle i^{l_1}Y_{l_1m_1}(\hat{\mathbf{r}})i^{-l_2}Y^*_{l_2m_2}(\hat{\mathbf{r}}')\ ,\end{aligned} \tag{2.19}$$

where $|n\rangle$ and E_n denote the nth state and its energy. Here we assumed the ground state has spin $J=0$ and isospin $T=0$. The radial part $\Pi_{Jl_1l_2a}(r,r';\omega)$ is given by

$$\Pi_{Jl_1l_2a}(r,r';\omega)=\langle 0|\left[\hat{j}^{\dagger}_{l_1JMa}(r)\frac{1}{\hbar\omega-(H-E_0)+i\eta}\hat{j}_{l_2JMa}(r')+\hat{j}_{l_2JMa}(r')\frac{1}{-\hbar\omega-(H-E_0)+i\eta}\hat{j}^{\dagger}_{l_1JMa}(r)\right]|0\rangle \ . \tag{2.20}$$

For the free polarization propagator, the intermediate states are the particle-hole states, and hence the radial part is written in a simple form

$$\Pi^0_{Jl_1l_2a}(r,r';\omega)=\sum_{ph}\phi^{Jl_1a*}_{ph}(r)\mathcal{D}^0_{ph}(\omega)\phi^{Jl_2a}_{ph}(r') \ , \tag{2.21}$$

where the suffices p and h denote the sets of the quantum numbers (l_p,j_p,ϵ_p,t_p) and (l_h,j_h,n_h,t_h), respectively. The energy denominator $\mathcal{D}^0_{ph}(\omega)$ is

$$\mathcal{D}^0_{ph}(\omega)=\frac{1}{\hbar\omega-(\epsilon_p-\epsilon_h)+i\eta}+\frac{1}{-\hbar\omega-(\epsilon_p-\epsilon_h)+i\eta} \tag{2.22}$$

and the radial part of the current expectation value is

$$\begin{aligned}\phi^{Jla}_{ph}(r)&=\langle[(l_pj_p\epsilon_pt_p)(l_hj_hn_ht_h)^{-1}]lJM|\hat{j}_{lJMa}(r)|0\rangle\\&=\mathcal{G}^{Jla}_{ph}\frac{f^*_{l_pj_p}(r,\epsilon_p)u_{n_hl_hj_h}(r)}{r^2} \ ,\end{aligned} \tag{2.23}$$

with the geometrical factor $\mathcal{G}^{Jla}_{ph}$

$$\mathcal{G}^{Jla}_{ph}=\langle(l_p\tfrac{1}{2})j_p,(l_h\tfrac{1}{2})j_h;J|(l_pl_h)l,(\tfrac{1}{2}\tfrac{1}{2})1;J\rangle\langle t_p|\tau_a|t_h\rangle\langle\tfrac{1}{2}\|\sigma\|\tfrac{1}{2}\rangle(-i)^{l+1}(-)^{l_h}\left[\frac{(2l_p+1)(2l_h+1)}{12\pi}\right]^{1/2}\begin{bmatrix}l_p & l_h & l\\ 0 & 0 & 0\end{bmatrix} . \tag{2.24}$$

Using the method of the previous subsection, the sum over the continuum-state energy ϵ_p in Eq. (2.21) can be replaced by the radial part of the single-particle Green's function $g^{\rm oc}$, and then Eq. (2.21) is rewritten as

$$\Pi^0_{Jl_1l_2a}(r,r';\omega)=\sum_{ph}\mathcal{G}^{Jl_1a*}_{ph}\frac{u_{n_hl_hj_h}(r)}{r^2}[g^{\rm oc}_{l_pj_p}(r,r';\hbar\omega+\epsilon_h)+g^{\rm oc}_{l_pj_p}(r',r;-\hbar\omega+\epsilon_h)]\mathcal{G}^{Jl_2a}_{ph}\frac{u_{n_hl_hj_h}(r')}{r'^2} \ . \tag{2.25}$$

Now let us take into account the internucleon interaction in terms of RPA with the ring approximation in which the exchange term is approximated by a contact interaction. Then the polarization propagator satisfies[30,32] the RPA equation

$$\Pi^{\rm RPA}_{Jl_1l_2a}(r,r';\omega)=\Pi^0_{Jl_1l_2a}(r,r';\omega)+\sum_{l_3l_4}\int_0^\infty r_1^2dr_1\int_0^\infty r_2^2dr_2\Pi^0_{Jl_1l_3a}(r,r_1;\omega)V_{Jl_3l_4}(r_1,r_2)\Pi^{\rm RPA}_{Jl_4l_2a}(r_2,r';\omega) \ . \tag{2.26}$$

Here we write the particle-hole interaction in the form

$$\begin{aligned}V&=\sum_{i<j}\int\frac{d^3\mathbf{k}}{(2\pi)^3}[V_L(k)(\sigma^i\cdot\hat{\mathbf{k}})(\sigma^j\cdot\hat{\mathbf{k}})+V_T(k)(\sigma^i\times\hat{\mathbf{k}})(\sigma^j\times\hat{\mathbf{k}})](\tau^i\cdot\tau^j)e^{i\mathbf{k}\cdot(\mathbf{r}_i-\mathbf{r}_j)}\\&=\tfrac{1}{2}\sum_a\sum_{JM}\sum_{ll'}\int_0^\infty r^2dr\int_0^\infty r'^2dr'V_{Jll'}(r,r')\hat{j}^{\dagger}_{lJMa}(r)\hat{j}_{l'JMa}(r') \ ,\end{aligned} \tag{2.27}$$

with the radial part $V_{Jll'}(r,r')$

$$V_{Jll'}(r,r')=\frac{2}{\pi}\int_0^\infty k^2 dk j_l(kr)V_{Jll'}(k)j_{l'}(kr') \tag{2.28}$$

and

$$V_{Jll'}(k)=a_{Jl}V_L(k)a_{Jl'}+V_T(k)(\delta_{ll'}-a_{Jl}a_{Jl'}) , \tag{2.29}$$

where $a_{Jl}\equiv\langle J010|l0\rangle$ and $j_l(x)$ is the lth spherical Bessel function. $V_L(k)$ and $V_T(k)$ denote the longitudinal and the transverse part of the particle-hole interaction, respectively. To get Eq. (2.29), the relation $(\boldsymbol{\sigma}^i\cdot\boldsymbol{\sigma}^j)=(\boldsymbol{\sigma}^i\cdot\hat{\mathbf{k}})(\boldsymbol{\sigma}^j\cdot\hat{\mathbf{k}})+(\boldsymbol{\sigma}^i\times\hat{\mathbf{k}})(\boldsymbol{\sigma}^j\times\hat{\mathbf{k}})$ is useful.

3. *Response functions*

The response function for the spin-isospin currents is defined as

$$R_{\mu a\nu b}(\mathbf{r},\mathbf{r}';\omega)\equiv\sum_n\langle 0|\hat{j}_{\mu a}(\mathbf{r})|n\rangle\langle n|\hat{j}^\dagger_{\nu b}(\mathbf{r}')|0\rangle \times\delta(\hbar\omega-(E_n-E_0)) , \tag{2.30}$$

which can be written by the spin-isospin polarization propagator as

$$R_{\mu a\nu b}(\mathbf{r},\mathbf{r}';\omega)=-\frac{1}{\pi}\mathrm{Im}\Pi_{\mu a\nu b}(\mathbf{r},\mathbf{r}';\omega) . \tag{2.31}$$

In order to compare our calculations with previous works, we define the response function in the momentum representation:

$$\tilde{R}_{\mu a\nu b}(\mathbf{q},\mathbf{q}';\omega)=\int d^3\mathbf{r}\int d^3\mathbf{r}' e^{i\mathbf{q}\cdot\mathbf{r}}R_{\mu a\nu b}(\mathbf{r},\mathbf{r}';\omega) \times e^{-i\mathbf{q}'\cdot\mathbf{r}'} . \tag{2.32}$$

Following the convention of Alberico *et al.*,[30] the longitudinal response $R_L(q,\omega)$ and the transverse response $R_T(q,\omega)$ are defined as

$$\begin{aligned}R_L(q,\omega)&\equiv\sum_n\langle 0|O_L(\mathbf{q})|n\rangle\langle n|O_L^\dagger(\mathbf{q})|0\rangle\delta(\hbar\omega-(E_n-E_0))\\&=\tfrac{1}{2}\sum_{\mu\nu}(-)^{\mu+\nu}q_{-\mu}q^*_{-\nu}\tilde{R}_{\mu z\nu z}(\mathbf{q},\mathbf{q};\omega)\\&=-\frac{1}{2\pi}\mathrm{Im}\sum_{Jl_1l_2}\frac{2J+1}{4\pi}a_{Jl_1}\Pi_{Jl_1l_2z}(q,q;\omega)a_{Jl_2} ,\end{aligned} \tag{2.33}$$

and

$$\begin{aligned}R_T(q,\omega)&\equiv\sum_n\langle 0|O_T(\mathbf{q})|n\rangle\langle n|O_T^\dagger(\mathbf{q})|0\rangle\delta(\hbar\omega-(E_n-E_0))\\&=\tfrac{1}{2}\sum_n\sum_{\mu\nu}\sum_{\mu'\nu'}q_{\mu'}q^*_{\nu'}\langle 1\mu 1\mu'|1n\rangle\langle 1\nu 1\nu'|1n\rangle\tilde{R}_{\mu z\nu z}(\mathbf{q},\mathbf{q};\omega)\\&=-\frac{1}{4\pi}\mathrm{Im}\sum_{Jl_1l_2}\frac{2J+1}{4\pi}\Pi_{Jl_1l_2z}(q,q;\omega)(\delta_{l_1l_2}-a_{Jl_1}a_{Jl_2}) ,\end{aligned} \tag{2.34}$$

where q_μ is the spherical tensor component of the momentum transfer $\mathbf{q}$, and the radial part $\Pi_{Jl_1l_2a}(q,q';\omega)$ is given by

$$\Pi_{Jl_1l_2a}(q,q';\omega)=(4\pi)^2qq'\int_0^\infty r^2dr\int_0^\infty r'^2dr' j_{l_1}(qr)\Pi_{Jl_1l_2a}(r,r';\omega)j_{l_2}(q'r') . \tag{2.35}$$

Note that both R_L and R_T are linear combinations of $\Pi_{Jl_1l_2z}$ and that the difference only comes from the geometrical factors $a_{Jl_1}a_{Jl_2}$ and $(\delta_{l_1l_2}-a_{Jl_1}a_{Jl_2})$.

B. Distorted-wave impulse approximation (DWIA)

1. *The nucleon-nucleon (NN) t matrix*

In DWIA, the interaction between the nucleon 0 in the projectile and the nucleon i in the target is given by the *NN* t matrix, the isospin-dependent part of which is written in the *NN* c.m. frame as

$$\begin{aligned}t_i(\mathbf{q})=&[\alpha-i\gamma\{(\boldsymbol{\sigma}^0\cdot\hat{\mathbf{n}})+(\boldsymbol{\sigma}^i\cdot\hat{\mathbf{n}})\}\\&+\beta(\boldsymbol{\sigma}^0\cdot\hat{\mathbf{n}})(\boldsymbol{\sigma}^i\cdot\hat{\mathbf{n}})+\delta(\boldsymbol{\sigma}^0\cdot\hat{\mathbf{q}})(\boldsymbol{\sigma}^i\cdot\hat{\mathbf{q}})\\&+\epsilon(\boldsymbol{\sigma}^0\cdot\hat{\mathbf{p}})(\boldsymbol{\sigma}^i\cdot\hat{\mathbf{p}})] ,\end{aligned} \tag{2.36}$$

where $\mathbf{q}=\boldsymbol{\kappa}'-\boldsymbol{\kappa}$, $\mathbf{n}=\boldsymbol{\kappa}\times\boldsymbol{\kappa}'$, $\hat{\mathbf{p}}=\hat{\mathbf{q}}\times\hat{\mathbf{n}}$, and $\boldsymbol{\kappa}$ and $\boldsymbol{\kappa}'$ are the momentum of the nucleon 0 in the initial and final channel, respectively. It is normalized as

$$d\sigma/d\Omega=\{\mu^2/(2\pi\hbar^2)^2/(2s+1)\}|t|^2$$

$$(\mu=\sqrt{m^2+(\kappa/c)^2}/2) .$$

The amplitudes α through ϵ are functions of q and the incident energy E.

In DWIA we need the t matrix in the c.m. frame of N-nucleus (NA), which is approximately given by

$$\langle \mathbf{k}_0';\mathbf{k}_i'|t_i|\mathbf{k}_0;\mathbf{k}_i\rangle_{NA}=\eta t_i(\mathbf{q}) , \tag{2.37}$$

with the Möller factor η

$$\eta=\left[\frac{E_N(\kappa')E_N(-\kappa')E_N(\kappa)_N(-\kappa)}{E_N(\mathbf{k}_0')E_N(\mathbf{k}_i')E_N(\mathbf{k}_0)E_N(\mathbf{k}_i)}\right]^{1/2} , \tag{2.38}$$

where $\mathbf{k}_j$ ($\mathbf{k}_j'$) is the momentum of the nucleon j in the incident (exit) channel in the NA c.m. system and $E_N(\mathbf{k})=[(mc^2)^2+(\hbar c\mathbf{k})^2]^{1/2}$. In this frame transformation we neglect spin rotation and use an approximation $\mathbf{q}=\mathbf{k}_0'-\mathbf{k}_0$ (exact in nonrelativistic limit). Following the optimum factorization and on-shell approximation of Picklesimer *et al.*,[33] η turns out to be effectively a function of only q and E.

First we note that the α term does not contribute to the excitation of the spin modes. Next if we assume

$$\begin{aligned}&\eta\beta=\eta\epsilon\equiv\mathcal{V}_T(q)\ \text{(transverse)} ,\\ &\eta\delta\equiv\mathcal{V}_L(q)\ \text{(longitudinal)} ,\\ &\gamma=0 ,\end{aligned} \tag{2.39}$$

the t matrix only depends on $\mathbf{q}$ and E and consequently can be expressed by the two components, the spin longitudinal and transverse, as

$$t_i(\mathbf{q})=\mathcal{V}_L(q)(\boldsymbol{\sigma}^0\cdot\hat{\mathbf{q}})(\boldsymbol{\sigma}^i\cdot\hat{\mathbf{q}})+\mathcal{V}_T(q)(\boldsymbol{\sigma}^0\times\hat{\mathbf{q}})(\boldsymbol{\sigma}^i\times\hat{\mathbf{q}}) , \tag{2.40}$$

because of the relation

$$(\boldsymbol{\sigma}^0\cdot\hat{\mathbf{n}})(\boldsymbol{\sigma}^i\cdot\hat{\mathbf{n}})+(\boldsymbol{\sigma}^0\cdot\hat{\mathbf{p}})(\boldsymbol{\sigma}^i\cdot\hat{\mathbf{p}})=(\boldsymbol{\sigma}^0\times\hat{\mathbf{q}})(\boldsymbol{\sigma}^i\times\hat{\mathbf{q}}) .$$

Then the t matrix in the $\mathbf{r}$ representation becomes local and is given by

$$\begin{aligned}\mathcal{V}(\mathbf{r}_i,\mathbf{r})&=\int\frac{d^3\mathbf{q}}{(2\pi)^3}t_i(\mathbf{q})^{-i\mathbf{q}\cdot(\mathbf{r}_i-\mathbf{r})}\\ &\equiv\sum_{\alpha=L,T}\mathcal{V}_\alpha(\mathbf{r}_i,\mathbf{r}) ,\end{aligned} \tag{2.41}$$

and in the spherical tensor representation as

$$\mathcal{V}_\alpha(\mathbf{r}_i,\mathbf{r})=\sum_{JM}\sum_{ll'}\mathcal{V}^\alpha_{Jll'}(r_i,r)[i^lY_l(\hat{\mathbf{r}}_i)\times\boldsymbol{\sigma}^i]^{J\dagger}_M \times[i^{l'}Y_{l'}(\hat{\mathbf{r}})\times\boldsymbol{\sigma}^0]^J_M , \tag{2.42}$$

where

$$\mathcal{V}^L_{Jll'}(r_i,r)=\frac{2}{\pi}\int_0^\infty q^2dq\, j_l(qr_i)a_{Jl}\mathcal{V}_L(q)a_{Jl'}j_{l'}(qr) , \tag{2.43}$$

$$\mathcal{V}^T_{Jll'}(r_i,r)=\frac{2}{\pi}\int_0^\infty q^2dq\, j_l(qr_i)\mathcal{V}_T(q) \times(\delta_{ll'}-a_{Jl}a_{jl'})j_{l'}(qr) . \tag{2.44}$$

Now the DWIA cross section $d^2\sigma/d\Omega\, d\omega$ can be calculated by utilizing the two-point polarization propagators as will be shown in Sec. II B 2.

Figure 2 shows the q dependence of β, δ, and ϵ given by Bugg and Wilkin[35] from the NN scattering data at the incident energy $E_p=515$ MeV in laboratory frame. It shows that the condition $\beta=\epsilon$ does not hold well though the q dependence of β and ϵ are similar. For technical reasons, we make the assumption (2.39) in the present calculation in order to localize the t matrix [i.e., to get the form (2.40)].

2. DWIA

The inclusive cross section $d^2\sigma/d\Omega\, d\omega$ of the nucleon-nucleus inelastic scattering is expressed by the scattering matrix T^{fi}_{n0} as

$$\begin{aligned}\frac{d^2\sigma}{d\Omega\, d\omega}&=\frac{\mu_i\mu_f}{(2\pi\hbar^2)^2}\frac{k_f}{k_i}\frac{1}{2s_i+1}\sum_n|T^{fi}_{n0}|^2\delta(\hbar\omega-(E_n-E_0))\\ &\equiv K\sum_n|T^{fi}_{n0}|^2\delta(\hbar\omega-(E_n-E_0)) ,\end{aligned} \tag{2.45}$$

where the relativistic reduced mass is defined as

$$\mu_{i(f)}\equiv\frac{E^{(p)}_{i(f)}E^{(t)}_{i(f)}}{c^2(E^{(p)}_{i(f)}+E^{(t)}_{i(f)})} , \tag{2.46}$$

and $E^{(p)}_{i(f)}$ are $E^{(t)}_{i(f)}$ are the initial (final) energy of the projectile and the target, respectively. The scattering matrix T^{fi}_{n0} is given by

$$T^{fi}_{n0}=\langle\chi^{(-)}_f(\mathbf{k}_f,\mathbf{r})\Phi_n(\mathbf{r}_1,\ldots,\mathbf{r}_A)|\sum_i\mathcal{V}(\mathbf{r}_i,\mathbf{r})|\chi^{(+)}_i(\mathbf{k}_i,\mathbf{r})\Phi_0(\mathbf{r}_1,\ldots,\mathbf{r}_A)\rangle , \tag{2.47}$$

where $\Phi_0(\mathbf{r}_1,\ldots,\mathbf{r}_A)$ and $\Phi_n(\mathbf{r}_1,\ldots,\mathbf{r}_A)$ are the wave function of the ground and the nth excited state, respectively, and $\chi^{(+)}_i(\mathbf{k}_i,\mathbf{r})$ and $\chi^{(-)}_f(\mathbf{k}_f,\mathbf{r})$ the incident and the outgoing distorted wave, respectively.

The sum in (2.45) can be rewritten as

$$\begin{aligned}\sum_n|T^{fi}_{n0}|^2\delta(\hbar\omega-(E_n-E_0))=&-\frac{1}{\pi}\mathrm{Im}\langle0|\sum_i\hat{S}^\dagger(\mathbf{r}_i)\frac{1}{\hbar\omega-(H-E_0)+i\eta}\sum_j\hat{S}(\mathbf{r}_j)\\ &+\sum_j\hat{S}(\mathbf{r}_j)\frac{1}{-\hbar\omega-(H-E_0)+i\eta}\sum_i\hat{S}^\dagger(\mathbf{r}_i)|0\rangle ,\end{aligned} \tag{2.48}$$

where

$$\hat{S}(\mathbf{r}_i)\equiv\int d^3\mathbf{r}\,\chi_f^{(-)*}(\mathbf{k}_f,\mathbf{r})\mathcal{V}(\mathbf{r}_i,\mathbf{r})\chi_i^{(+)}(\mathbf{k}_i,\mathbf{r})\ . \tag{2.49}$$

For the optical potential with a spin-orbit force, the distorted wave $\chi_i^{(+)}(\mathbf{k}_i,\mathbf{r})$ is expressed by[34]

$$\begin{aligned}\chi_i^{(+)}(\mathbf{k}_i,\mathbf{r})&=\sum_{m_{s_i}'}\chi^{(+)}_{m_{s_i}'m_{s_i}}(\mathbf{k}_i,\mathbf{r})|m_{s_i}'t_i\rangle\\&=\frac{4\pi}{k_i r}\sum_{l_i m_i m_i'}\sum_{j_i m_{s_i}' m_{s_i}}\langle l_i m_i s m_{s_i}|j_i m_{j_i}\rangle Y^*_{l_i m_i}(\hat{\mathbf{k}}_i)\langle l_i m_i' s m_{s_i}'|j_i m_{j_i}\rangle Y_{l_i m_i'}(\hat{\mathbf{r}})i^{l_i}e^{i\sigma_l}u^{(+)}_{l_i j_i}(k,r)|m_{s_i}'t_i\rangle\ ,\end{aligned} \tag{2.50}$$

where σ_l is Coulomb phase shift and $u_{lj}^{(+)}$ has the asymptotic behavior

$$u_{lj}^{(+)}(k,r)\sim\sin\left[kr-\eta_C\ln 2kr-\frac{l\pi}{2}+\sigma_l\right]\ , \tag{2.51}$$

with $\eta_C=Z_tZ_pe^2\mu/\hbar^2k$. Substituting (2.42) and (2.50) into (2.49), we obtain the spherical tensor representation of $\hat{S}$:

$$\hat{S}(\mathbf{r}_i)=\sum_{\alpha=L,T}\sum_{lJMa}\sum_{m_{s_f}m_{s_i}}s^{\alpha m_{s_f}m_{s_i}}_{lJMa}(r_i)[i^lY_l(\hat{\mathbf{r}}_i)\times\boldsymbol{\sigma}^i]^J_M\tau^i_a\ , \tag{2.52}$$

where

$$s^{\alpha m_{s_f}m_{s_i}}_{lJMa}(r)\equiv\sum_{l'}\int_0^\infty r'^2dr'\mathcal{V}^\alpha_{Jll'}(r,r')f^{m_{s_f}m_{s_i}}_{l'JMa}(\mathbf{k}_i,\mathbf{k}_f;r')\quad(\alpha=L,T) \tag{2.53}$$

and

$$\begin{aligned}f^{m_{s_f}m_{s_i}}_{lJMa}(\mathbf{k}_i,\mathbf{k}_f;r)&\equiv\sum_{m_{s_f}'m_{s_i}'}\int d\Omega_{\mathbf{r}}\chi^{(-)*}_{m_{s_f}'m_{s_f}}(\mathbf{k}_f,\mathbf{r})\langle m_{s_f}'t_f|[i^lY_l(\hat{\mathbf{r}})\times\boldsymbol{\sigma}]^J_M\tau_a|m_{s_i}'t_i\rangle\chi^{(+)}_{m_{s_i}'m_{s_i}}(\mathbf{k}_i,\mathbf{r})\\&=\frac{\sqrt{24\pi}}{k_ik_fr^2}\sqrt{(2J+1)(2l+1)}\sum_{l_ij_i}\sum_{l_fj_f}i^{l_i+l-l_f}e^{i(\sigma_{l_f}+\sigma_{l_i})}\\&\quad\times u^{(+)}_{l_fj_f}(k_f,r)u^{(+)}_{l_ij_i}(k_i,r)(2l_i+1)\sqrt{(2j_i+1)(2l_f+1)}\langle l_i0l0|l_f0\rangle\\&\quad\times\begin{Bmatrix}l_f&s_f&j_f\\l_i&s_i&j_i\\l&1&J\end{Bmatrix}\langle l_i0s_im_{s_i}|j_im_{s_i}\rangle\langle l_fm_fs_fm_{s_f}|j_fm_{s_i}+M\rangle\\&\quad\times\langle j_im_{s_i}JM|j_fm_{s_i}+M\rangle\langle t_f|\tau_a|t_i\rangle(-)^{(m_f+|m_f|)/2}\left[\frac{(l_f-|m_f|)!}{(l_f+|m_f|)!}\right]^{1/2}P^{|m_f|}_{l_f}(\cos\theta)\ ,\end{aligned} \tag{2.54}$$

where $\mathbf{k}_i$ is taken to be parallel to the z axis and θ is the scattering angle.

Using $\hat{j}_{lJMa}(r)$ of Eq. (2.18), the expression

$$\sum_i\hat{S}(\mathbf{r}_i)=\sum_\alpha\sum_{lJMa}\sum_{m_{s_f}m_{s_i}}\int_0^\infty s^{\alpha m_{s_f}m_{s_i}}_{lJMa}(r)\hat{j}_{lJMa}(r)r^2dr \tag{2.55}$$

is obtained. Thus we obtain the final expression for the cross section:

$$\begin{aligned}\frac{d^2\sigma}{d\Omega\,d\omega}&=-K\frac{1}{\pi}\mathrm{Im}\sum_a\sum_{JM}\sum_{l_1l_2}\sum_{m_{s_f}m_{s_i}}\sum_{\alpha\beta}\int_0^\infty r^2dr\int_0^\infty r'^2dr's^{\alpha m_{s_f}m_{s_i}*}_{l_1JMa}(r)\Pi_{Jl_1l_2a}(r,r';\omega)s^{\beta m_{s_f}m_{s_i}}_{l_2JMa}(r')\\&\equiv\sum_{\alpha,\beta=L,T}\sigma_{\alpha\beta}\ .\end{aligned} \tag{2.56}$$

Hereafter in this paper, we especially examine the diagonal parts

$$\sigma_L \equiv \sigma_{LL}, \quad \sigma_T \equiv \sigma_{TT} , \tag{2.57}$$

which correspond to the response functions R_L and R_T, respectively. Hence we call σ_L and σ_T the isovector spin longitudinal and transverse cross section, respectively. The nondiagonal parts, σ_{LT} and σ_{TL}, come from the mixing of the spin longitudinal and transverse modes. They vanish in the nuclear matter limit, and hence they are expected not to be large in finite nuclei. Note that σ_L and σ_T also include effects of the mixing.

In order to see the effect of the distortion, we give the expression of the PWIA cross section, which is simply written by R_L or R_T as

$$\sigma_\alpha^{\mathrm{PWIA}} = 2K|\mathcal{V}_\alpha(q)|^2 R_\alpha(q,\omega) \quad (\alpha = L,T) . \tag{2.58}$$

III. ISOVECTOR SPIN LONGITUDINAL AND TRANSVERSE RESPONSE FUNCTIONS

Here we give the numerical analysis of the isovector spin longitudinal and transverse response functions, $R_L(q,\omega)$ and $R_T(q,\omega)$ for ^{40}Ca by means of OCRPA in the ring approximation.

We used the single-particle potential

$$U(r) = -(V+iW)\frac{1}{1+\exp\left[\dfrac{r-R}{a}\right]} - 2\left[\frac{\hbar}{m_\pi c}\right]^2 \frac{V_{ls}}{a}\frac{\exp\left[\dfrac{r-R}{a}\right]}{r\left[1+\exp\left[\dfrac{r-R}{a}\right]\right]^2}(\boldsymbol{l}\cdot\mathbf{s}) + V_{\mathrm{Coul}} \tag{3.1}$$

with $R = r_0 A^{1/3}$, $r_0 = 1.27$ fm, $a = 0.67$ fm (Ref. 36), and $V_{ls} = 10.0$ MeV. V_{Coul} is the Coulomb potential of the uniformly charged sphere with the Coulomb radius parameter r_C set to be r_0. The real potential depth V is determined to give the observed separation energy of the most weakly bound states; $V = 54.8$ MeV for the proton and $V = 54.5$ MeV for the neutron in the present case. The imaginary potential depth W is set to zero for the occupied(hole) states. For the particle states $W = 5.0$ MeV is used in most calculations. The reason for the inclusion of the imaginary potential will be discussed later. The value corresponds to the value of the optical potential at the energy ~ 50 MeV. We also include the Δ-hole configuration. For Δ, $V = 30$ MeV and $W = V_{ls} = 0.0$ MeV are used.

For the effective particle-hole interaction, we adopted the $(\pi+\rho+g')$ model,[1] in which $V_L(q,\omega)$ and $V_T(q,\omega)$ of Eq. (2.27) are given by

$$V_L(q,\omega) = \frac{f^2}{m_\pi^2}\left[g' + \frac{q^2}{\omega^2-(q^2+m_\pi^2)}\Gamma_\pi^2(q,\omega)\right] , \tag{3.2}$$

$$V_T(q,\omega) = \frac{f^2}{m_\pi^2}\left[g' + C_\rho\frac{q^2}{\omega^2-(q^2+m_\rho^2)}\Gamma_\rho^2(q,\omega)\right] , \tag{3.3}$$

where m_π (=139 MeV) and m_ρ (=770 MeV) are the pion and ρ-meson masses, respectively, and C_ρ (=2.18) is the ratio of the ρ and π coupling, and $f^2/4\pi\hbar c = 0.08$ is the πNN coupling constant. The vertex form factors are given by

$$\Gamma_\pi(q,\omega) = \frac{\Lambda_\pi^2 - m_\pi^2}{\Lambda_\pi^2 - \omega^2 + q^2} , \tag{3.4}$$

$$\Gamma_\rho(q,\omega) = \frac{\Lambda_\rho^2 - m_\rho^2}{\Lambda_\rho^2 - \omega^2 + q^2} , \tag{3.5}$$

with $\Lambda_\pi = 1300$ MeV and $\Lambda_\rho = 2000$ MeV. From Eqs. (3.2) and (3.5) we used the convention $\hbar = c = 1$. The interaction for Δ is obtained by replacing σ, τ, and f by the standard spin and isospin transition operator $\mathbf{S}$ and $\mathbf{T}$ and the $\pi N\Delta$ coupling constant $f^* = 2.0f$ for each $N\Delta\pi(\rho)$ vertex. The constant g' is chosen to be the same for N and Δ couplings, the universality ansatz, though it is questioned.[13,37] We summed up over the total angular momentum J up to 11 [see Eqs. (2.33) and (2.34)].

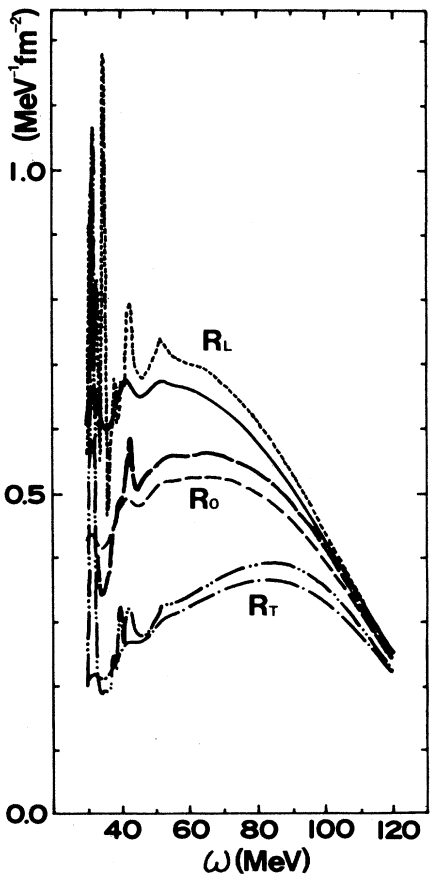

FIG. 3. Response functions by OCRPA. The results of $W = 0.0$ MeV and 5.0 MeV are compared. The results of R_L, R_0, and R_T are denoted by the solid (the dotted), the short-dashed (the long-dashed) and the dash-dot (the dash-dot-dot) lines for $W = 5.0$ MeV (0.0 MeV), respectively.

Figures 3 and 4 show the energy spectra of the response functions at $q=1.75$ fm^{-1} with $g'=0.6$. The isovector spin longitudinal and transverse response functions with the nuclear correlation (RPA) are denoted by R_L and R_T, respectively, while those without correlation (free response) R_L^0 and R_T^0, are both denoted by R_0 without distinguishing them because they are extremely close to each other. In principle the single-particle spin-orbit force makes R_L^0 and R_T^0 different, but not in the actual calculation.

In Fig. 3 the results for $W=0.0$ MeV and $W=5.0$ MeV are compared. Many sharp resonances are seen at lower ω for $W=0.0$ MeV. This is because the spreading width is completely neglected in this case. We know of no reasonable way to incorporate the spreading width in the framework of the continuum RPA. A prescription sometimes used is to introduce the imaginary potential for the particle state.[26] This forces us to use OCRPA. By setting $W=5.0$ MeV, the sharp structures are well smeared out but it also affects the strength of the responses, i.e., the strength is reduced in the peak region. Structures still remain in the low-energy region with about 10 MeV width. One must note that the energy integrated response depends on W in the present prescription.

The results are very close to those of the continuum RPA calculation by Shigehara *et al.*,[18] who did not use g' but used $\pi+\rho$ exchange potential with the short range cutoff at $r_c=0.7$ fm as the effective p-h interaction. This implies our choice $g'=0.6$ corresponds to their interaction. Considering that the phenomenological analyses suggest $g'\approx 0.6$–0.7, we keep $g'=0.6$ for all calculations in this paper except when a different g' is explicitly mentioned.

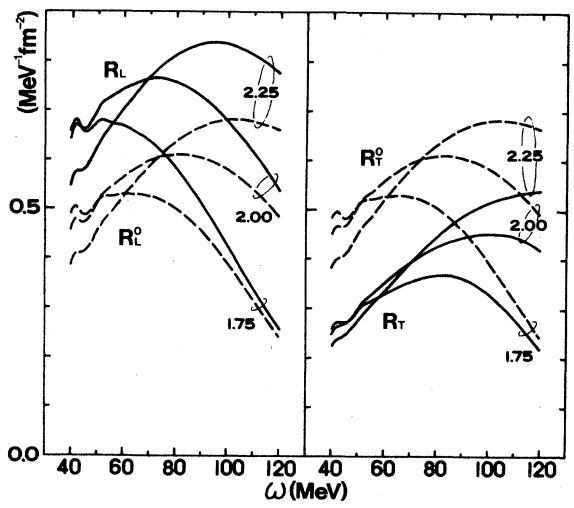

FIG. 5. The energy spectra of the response functions R_L and R_T (the solid lines) and R_L^0 and R_T^0 (the dashed lines) for fixed transferred momenta $q=1.75$, 2.00, and 2.25 fm^{-1} are shown. Note that in Figs. 3 and 4 the uncorrelated response functions R_L^0 and R_T^0 are denoted by R_0 without distinction (see the text).

In Fig. 4 we compare the results of $W=5.0$ MeV with those of the Fermi gas model with the Fermi momentum $k_F=1.20$ fm^{-1}. We see that the Fermi gas model overestimates the enhancement of R_L at lower ω very much, and find that the original prediction of the large enhancement of R_L is simply an artifact of the Fermi gas model.

The transferred momentum q dependence of the energy spectra is shown in Fig. 5. We clearly see the softening

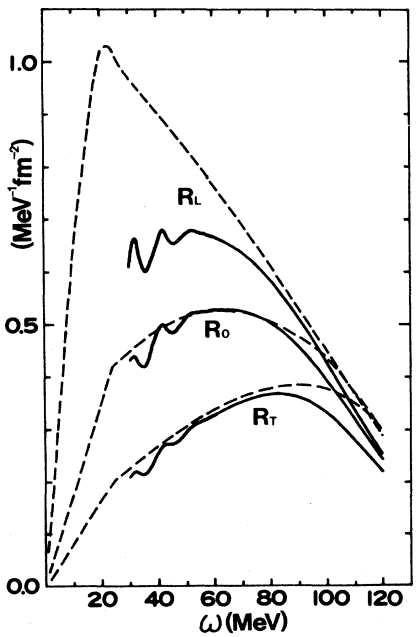

FIG. 4. Response functions in the Fermi gas model with $k_F=1.2$ fm^{-1} (dashed lines) are compared with those of OCRPA (the solid lines).

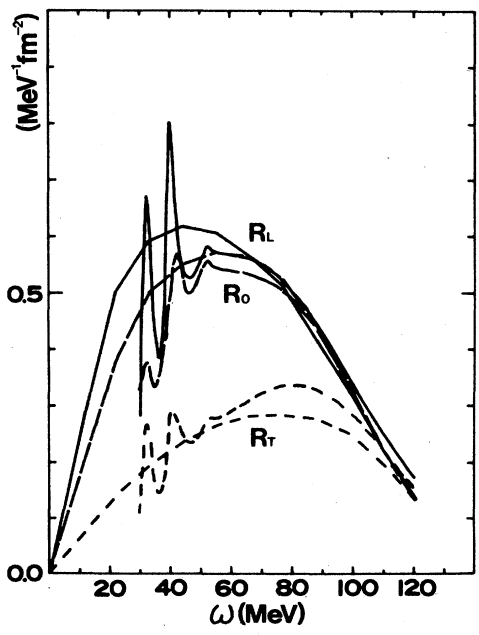

FIG. 6. Response functions of the bound-state approximation (Ref. 14) are compared with those of OCRPA at $q=330$ MeV/$c=1.67$ fm^{-1}. The solid, the long-dashed, and the dashed lines denote R_L, R_0, and R_T, respectively.

(hardening) and the enhancement (quenching) of R_L (R_T) over a range of q. It is found that the trajectory of the peak of R_0 lies on the quasifree peak line $\omega=q^2/2m$, because the single-particle potential we used is velocity independent except for the spin-orbit force whose effects were seen to be very small. However, we note that the peaks of the response functions are so broad that the peak position is sensitive to models employed.

In Fig. 6 the response functions at $q=330$ MeV calculated in the bound-state approximation by Alberico *et al.*[14] are compared with our OCRPA results. Alberico *et al.* used $g'=0.7$ with the form factor $\Gamma_\pi(q,\omega)$. It corresponds to $g'=0.61$ in our calculation which does not have Γ_π. Thus we compare their results with ours for $g'=0.61$. Those approximations seem to work only qualitatively. Getting more quantitative results in these approximations could become rather elaborate[38] especially in the quasifree region.

IV. DWIA CALCULATION

In this section we give the spin longitudinal and transverse cross sections, σ_L and σ_T, defined in Eq. (2.57) calculated in terms of DWIA for the reaction ^{40}Ca(p,p') at $E_p=500$ MeV and compare the results with the polarization transfer experiment at LAMPF (Ref. 10) in the next section. We also discuss the dependence on the transferred multipolarity and on the hole states.

The optical potential used both for the incident and the exit channel is the set 4 of the Dirac phenomenological potential obtained by Clark *et al.*[39] We used the *NN t* matrix obtained by Bugg and Wilkin[35] at $E_p=515$ MeV.

For the calculation of σ_L, we equate [Eq. (2.39)]

$$\mathcal{V}_L(q)=\eta\delta(q) \ . \tag{4.1}$$

To calculate σ_T, however, we need the condition $\beta=\varepsilon$ which is not fully satisfied. So we used the following prescription. First we calculate the two cross sections by setting

$$\mathcal{V}_T(q)=\eta\beta(q) \text{ and } \eta\varepsilon(q) \ , \tag{4.2}$$

respectively. Then, their average is presented as σ_T. We approximate the Jacobian η to be constant ($\eta^2=0.75$) since it varies only very slightly in the whole region of q and ω in our analysis.

In Fig. 7 we show the energy spectra of the cross sections, σ_L and σ_T, at the scattering angles $\theta_{\text{c.m.}}=19.2°$, 21.7°, and 24.2°, which approximately correspond to the momentum transfer $q=1.75$, 1.96, and 2.18 fm^{-1}. The angle of the center-of-mass system, $\theta_{\text{c.m.}}=19.2°$, corresponds to that of the laboratory frame, $\theta_{\text{lab}}=18.5°$, the angle of the LAMPF experiment. The full lines denote the cross sections with the RPA correlation, $\sigma_\alpha^{\text{RPA}}$, ($\alpha=L,T$), and the dashed lines represent those without the nuclear correlation, σ_α^0, ($\alpha=L,T$). For a fixed angle one sees all the peaks of $\sigma_\alpha^{\text{RPA}}$ and σ_α^0 ($\alpha=L,T$) lie at almost the same energy which is about 10 MeV below the quasifree peak $\omega=q^2/2m$. However, the enhancement in σ_L and the quenching in σ_T can still be seen.

In Fig. 8 the energy spectra of the cross sections calculated by PWIA and DWIA at $\theta_{\text{c.m.}}=21.7°$ are compared

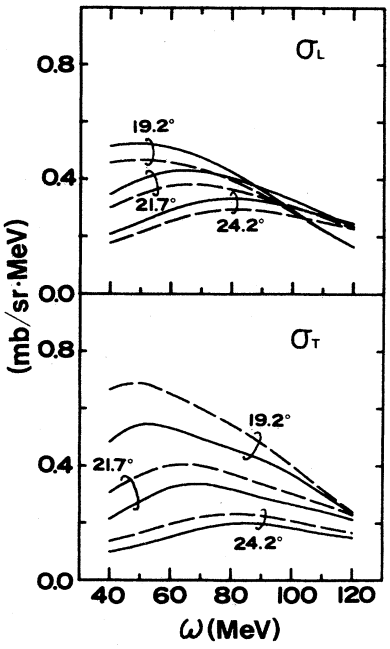

FIG. 7. The energy spectra of the cross sections, σ_L, and σ_T, at the scattering angles $\theta_{\text{c.m.}}=19.2°$, 21.7°, and 24.2°. The solid and the dashed lines represent the RPA and uncorrelated cross sections, respectively.

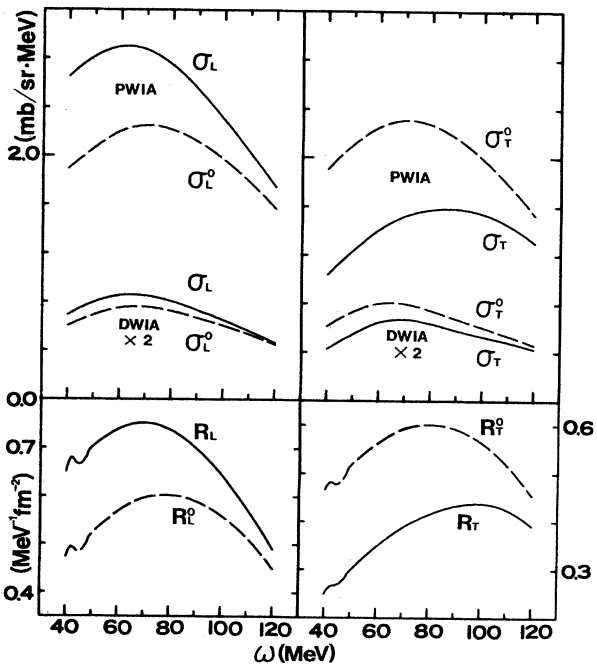

FIG. 8. The energy spectra of the cross sections, σ_L and σ_T, obtained by PWIA and DWIA at $\theta_{\text{c.m.}}=21.7°$ are compared with the response functions at $q=1.96$ fm^{-1}. The DWIA cross sections are multiplied by a factor 2. The solid and the dashed lines represent the RPA and the uncorrelated results.

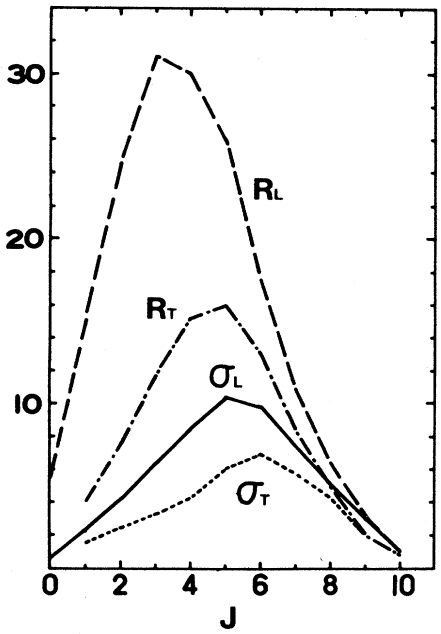

FIG. 9. The contribution of each J to R_L and R_T at $q=1.75$ fm^{-1} and to σ_L and σ_T at $\theta_{\text{c.m.}}=19.2°$ for $\omega=60$ MeV are shown. R_L (dashed) and σ_L (solid) [R_T (dash-dot) and σ_T (dotted)] are normalized to be 1.00 (0.768) at $J=10$, respectively.

with those of the response functions at $q=1.96$ fm^{-1}. The reduction of the cross sections due to the absorption (a factor 5–7 in the present case) is clearly seen. In the PWIA expression (2.58), the kinematical factor K shifts the peak of the energy spectra downwards about 10 MeV in going from the response functions to the cross section. For the RPA case, an extra downwards shift in the transverse mode and an upward shift in the longitudinal mode are seen. They are ascribed to the effect of distortion which almost diminishes the softening and hardening due to the nuclear correlation. Previous Glauber approximation calculations have also shown qualitatively similar results. Note that the peak positions of cross sections are lower than those of the surface response functions partly due to the ω dependence of the factor K of (2.45).

The surface response calculations of Alberico *et al.*[5]

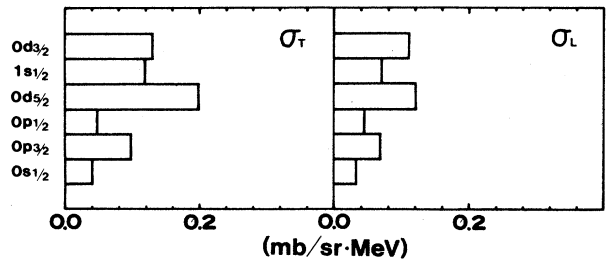

FIG. 10. The cross sections $\sigma^0_L(h)$ and $\sigma^0_T(h)$, the contributions from the different hole states, at $\theta_{\text{c.m.}}=19.2°$ for $\omega=60$ MeV are compared.

TABLE I. The attenuation factor $\sigma^0_\alpha(h)/R_0(h)$ $(\alpha=L,T)$. They are normalized for the $1s_{1/2}$ state.

Holes	Transverse	Longitudinal
$0d_{3/2}$	0.688	0.858
$1s_{1/2}$	1.000	1.000
$0d_{5/2}$	0.701	0.823
$0p_{1/2}$	0.415	0.584
$0p_{3/2}$	0.413	0.542
$0s_{1/2}$	0.238	0.345

and Shigehara *et al.*[18] did not show the shift of the peak position, but only an attenuation of the strength. We do not know the reason for this difference but it may be due to the replacement of the impact parameter b by the radius r to get the damping function $F(b)$ in the Glauber theory.

In order to see the effects of the distortion in more detail, we investigated the dependence on the transferred angular momentum, J, both of the response functions and the cross sections. Figure 9 shows the contributions of each J to R_L and R_T at $q=1.75$ fm^{-1} and to σ_L and σ_T at $\theta_{\text{c.m.}}=19.2°$ for the excitation energy $\omega=60$ MeV. In the figure $R_L(J=10)$ and $\sigma_L(J=10)$ are normalized to unity while $R_T(J=10)$ and $\sigma_T(J=10)$ are set to be 0.768, the value of $R_T(10)/R_L(10)$. As is expected, the smaller J are more attenuated. Hence, the dominant multipolarities become larger for the cross sections than for the response functions. The most important multipolarity is $J=3$ (5) for R_L (R_T), but $J=5$ (6) for σ_L (σ_T) at this ω and $q(\theta)$. For larger q with the same ω, it moves to the higher J. These features are consistent with the expectation for a surface reaction.

We also investigated the contribution from the different hole states. Since one cannot separate the contributions from the individual hole state in RPA, we carried out this analysis only for the uncorrelated case, namely for R_0 and $\sigma^0_{L(T)}$. The histogram of the cross sections, $\sigma^0_{L(T)}(h)$, the contribution from the hole state h at $\omega=60$ MeV and $\theta=19.2°$, are shown in Fig. 10, and the attenuation factors due to the absorption

$$\sigma^0_\alpha(h)/R_0(h) \quad (\alpha=L,T) \tag{4.3}$$

are presented in Table I (normalized for the $1s_{1/2}$ state). One sees that the absorption reduces the contribution from the deeper states very much. The gap of the attenuation between the major shells is also seen. However, the contributions from the deeper shells are still appreciable in spite of the surface natures of the reaction.

V. COLLECTIVITY RATIO

Now let us compare our results with the LAMPF data.[9,10] For this purpose, we introduce the collectivity ratio in the isovector channel as

$$r_1=\frac{R_L/R_L^0}{R_T/R_T^0}=\frac{R_L}{R_T}\ , \tag{5.1}$$

where for the second equality we used the fact that the

spin longitudinal and transverse free response functions, R_L^0 and R_T^0, are well approximated by $R_L^0 = R_T^0 = R_0$ as was mentioned in Sec. III. Assuming that the isoscalar responses are noncollective and can be approximated by R_0, Rees *et al.*[10] introduced the ratio which includes both the isoscalar and the isovector contributions as

$$r_{1+0} = \frac{(3.62R_L + R_0)/4.62}{(1.15R_T + R_0)/2.15} = \frac{(3.62r_1 + 1)/4.62}{(1.15r_1 + 1)/2.15} . \quad (5.2)$$

Here $|\delta|^2/|\delta_0|^2 = 3.62$ and $|\varepsilon|^2/|\varepsilon_0|^2 = 1.15$ at $q = 1.75$ fm^{-1} and $E_p = 500$ MeV are used where δ_0 and ε_0 are the isoscalar correspondents of δ and ε, respectively. If PWIA were valid, r_{1+0} could be compared with the experimental data. However, this is not the case. To evaluate the effects of the distortion, the best we can do at the moment is to replace the ratios r_1 and r_{1+0}, by the ratios

$$r_1^D = \frac{\sigma_L^{\mathrm{RPA}}/\sigma_L^0}{\sigma_T^{\mathrm{RPA}}/\sigma_T^0} , \quad (5.3)$$

and

$$r_{1+0}^D = \frac{(3.62r_1^D + 1)/4.62}{(1.15r_1^D + 1)/2.15} . \quad (5.4)$$

In Fig. 11 the collectivity ratios r_1, r_{1+0}, r_1^D, and r_{1+0}^D at $q = 1.75$ fm^{-1} ($\theta_{\mathrm{c.m.}} = 19.2°$) are compared with the "experimental" results of LAMPF. Due to the effects of the finiteness the ratio r_1 is very much smaller than the original Fermi gas prediction, but still larger than the experimental results. The ratio r_{1+0}^D is similar to those previously obtained.[5,10–21] Comparing with the results of the SIS analysis[12,10] of LDA (Ref. 13) and of the surface response treatment of Alberico *et al.*[15,5] and Shigehara *et al.*,[18] our advanced treatment of the distortion reduces the ratio r^D more. Based on the SIS analysis, Rees *et al.*[10] claimed that a much larger g' was needed (e.g., $g' = 0.9$), but a more elaborate treatment of the distortion may not require such a larger value.

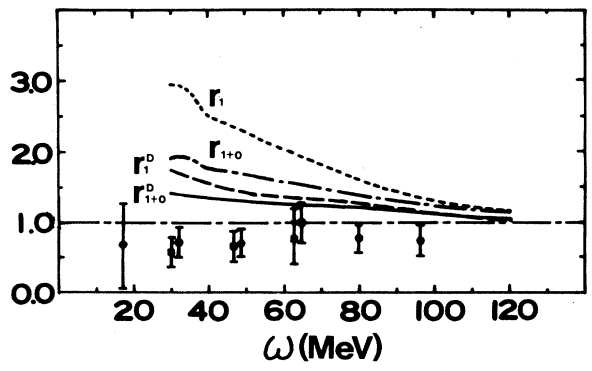

FIG. 11. The collectivity ratios r_1 (dotted) and r_{1+0} (dash-dot) at $q = 1.75$ fm^{-1}, and r_1^D (dashed) and r_{1+0}^D (solid) at $\theta_{\mathrm{c.m.}} = 19.2°$ are compared with the "experimental" results of LAMPF (Ref. 10).

VI. DISCUSSIONS

The present approach is not the final one. There remain many problems to be solved both on the nuclear structure and the reaction sides. We adopted the RPA approach. Effects of the 2p-2h components not included in RPA should be examined since their importance has long been known.[14,40] The validity of the ring approximation must be checked. Recently Shigehara[19] carried out RPA calculations which fully include the exchange effect and showed that the ring approximation is reasonable for the isovector spin modes, if one chooses suitable values of g'. The choice of the p-h effective interaction is also an open question, especially the results are sensitive to the value of g'. Just for technical reasons the universality ansatz, $g'_{NN} = g'_{N\Delta} = g'_{\Delta\Delta}$, has been used in the present analysis, but the ansatz has been challenged[13,37] and must be taken out.

The single-particle potential should, in principle, be the Hartree-Fock field obtained from the same interaction used in RPA. Such a totally self-consistent treatment is rather involved. The nonlocal Hartree-Fock field is often approximated by a local potential with the effective mass, m^*. As the expression for the energy of the quasifree peak $q^2/2m^*$ suggests, the energy spectrum of the response function may be affected very much by m^*. However, one must note that m^* itself depends on the energy and the density (hence the radius).[41] It is not easy to take into account these facts in the framework of OCRPA. In the present analysis, we simply used the Woods-Saxon potential as the mean field and did not introduce the effective mass.

In OCRPA the escape width is properly treated but the spreading width is not. It is well known that in the p-h modes the spreading widths of the particle states, of the hole states, and of the interference term mutually interfere and that this problem is a subtle and mode-dependent issue for the resonances.[42] The situation around the quasifree peak has not been investigated. Unfortunately, no good way is known to include the spreading width in the framework of the continuum RPA. What we did is only to simulate the spreading width effect in terms of the imaginary potential for the particle states as is sometimes done.[26]

In the present DWIA calculation, we imposed the condition $\beta = \varepsilon$ on the t matrix, which must be relaxed especially for the analysis of the spin observables. Once the condition is taken out, the t matrix becomes velocity dependent (essentially nonlocal). Then, one must prepare the response functions, one or both of whose vertices are associated with the velocity-dependent operators such as $[\sigma \times [Y_l(\hat{\mathbf{r}}) \times Y_{l'}(\hat{\mathbf{p}})]^L]^J_M$. This makes the problem very complicated. Anyway one must compare the experimental and the theoretical D_{ij} directly instead of the ratio R_L/R_T since an unjustified theory is involved to reduce the ratio.

For the analysis of the (p,p') reaction, more realistic treatment of the isoscalar contribution seems needed,[5,44] which may make the collectivity ratio smaller than unity.

The choice of the reference frame[21,43] and the treatment of the off-shell of the t matrix are common problems of DWIA. The relativistic effects, the choice of the

optical potential, etc. are other subjects to be studied. Finally the validity of DWIA itself should also be questioned.

VII. SUMMARY

In this paper we presented the detailed formalism of the continuum RPA with the orthogonality condition (OCRPA). It is then possible to take into account the finite size of the nucleus, the continuum nature of the single-particle states and the damping of the particle states. We also gave the detailed formula for the DWIA cross sections in terms of the response functions obtained by OCRPA. Using these methods we went much beyond the previous analysis on the spin-isospin modes in the quasifree scattering region.

By means of OCRPA we calculated the isovector spin longitudinal and transverse response functions, R_L and R_T, in a wide range of the energy $\omega \approx 30-120$ MeV and momentum $q \simeq 1.5-2.5$ fm^{-1} for ^{40}Ca. We confirmed the results of the previous works that the large enhancement and softening of R_L in the Fermi gas model are simply artifacts of the model.

The bound-state approximation for RPA is found to work reasonably well (at least qualitatively). The response functions are calculated in the angular momentum representation and it is found that the contribution from the modes with the angular momentum J must be summed up to about $J \approx 10$ in the present energy-momentum region. As q increases, the higher J becomes relatively more important.

Our major advance from the previous works is that a fully quantum-mechanical DWIA calculation was carried out for the response functions solved in the r space by OCRPA. We calculated the spin longitudinal and transverse cross sections, σ_L and σ_T, for ^{40}Ca(p,p') at $E_p = 500$ MeV for various angles.

The energy spectra of σ_L and σ_T for fixed angles obtained by DWIA and PWIA are compared with R_L and R_T. First we note that the kinematical factor shifts the peak drastically. It is found that not only the magnitude but also the shape of the spectra are appreciably affected by the distortion.

Because of the absorption, the contributions from the lower J modes are attenuated more strongly and thus the important J's are shifted upwards relative to those of the response functions. We found that the collectivity due to the nuclear correlation is much reduced by the absorption but the enhancement in the spin longitudinal mode and the quenching in the spin transverse mode still remain. In spite of the surface character of the reaction, we found that the contributions from the deeper hole states such as the $0s_{1/2}$ hole in ^{40}Ca are still non-negligible.

We compared the ratio R_L/R_T of LAMPF experimental results with our collectivity ratio $(\sigma_L^{\mathrm{RPA}}/\sigma_L^0)/(\sigma_T^{\mathrm{RPA}}/\sigma_L^0)$. The combined effects of the finiteness and of the distortion reduced the ratio from the original Fermi gas prediction but it is still slightly larger than unity, contrary to the experimental ratio (≤ 1). Comparing to the previous analysis by means of SIS and the surface response approaches, the reduction due to the distortion seems a little larger. To estimate the value of g' through such experiments, a fully quantum DWIA calculation is needed. Many remaining problems are pointed out for future investigation.

ACKNOWLEDGMENTS

M.I. thanks Nordisk Institut for Teoretisk Atomfysik (NORDITA) for the financial support for his stay in LUND and his thanks are also due to I. Hamamoto for her kind hospitality and valuable discussion during his stay in LUND. We appreciate valuable discussions with B. Mottelson, C. Ellegaard, and A. Brockstedt. The computer calculation for this work has been financially supported in part by the Research Center for Nuclear Physics (RCNP), Osaka University.

[1]W. M. Alberico, M. Ericson, and A. Molinari, Nucl. Phys. **A379**, 429 (1982); M. Ericson, *Proceedings of the International Conference on Spin Excitations in Nuclei,* edited by F. Petrovich *et al.* (Plenum, New York, 1984), p. 27.
[2]W. M. Alberico, M. Ericson, and A. Molinari, Phys. Lett. **92B**, 153 (1980).
[3]I. Bergqvist *et al.*, Nucl. Phys. **A469**, 648 (1987).
[4]C. Gaarde, Nucl. Phys. **A478**, 475c (1988).
[5]W. M. Alberico *et al.*, Phys. Rev. C **38**, 109 (1988).
[6]J. S. O'Connell and B. Schröder, Phys. Rev. C (to be published).
[7]R. E. Chrien *et al.*, Phys. Rev. C **21**, 1014 (1980).
[8]T. Jørgenssen *et al.* (private communication); C. Ellegaard *et al.*, Phys. Rev. Lett. **59**, 974 (1987).
[9]T. A. Carey *et al.*, Phys. Rev. Lett. **53**, 144 (1984).
[10]L. B. Rees *et al.*, Phys. Rev. C **34**, 627 (1986).
[11]W. M. Alberico *et al.*, Phys. Rev. C **30**, 1776 (1984).
[12]H. Esbensen, H. Toki, and G. F. Bertsch, Phys. Rev. C **31**, 1816 (1985).
[13]E. Shiino, Y. Saito, M. Ichimura, and H. Toki, Phys. Rev. C **34**, 1004 (1986).
[14]W. M. Alberico *et al.*, Phys. Rev. C **34**, 977 (1986).
[15]W. M. Alberico *et al.*, Phys. Lett. B **183**, 135 (1987).
[16]Y. Okuhara *et al.*, Phys. Lett. B **186**, 113 (1987).
[17]G. Chanfray, Nucl. Phys. **A474**, 114 (1987).
[18]T. Shigehara, K. Shimizu, and A. Arima, Nucl. Phys. **A477**, 583 (1988).
[19]T. Shigehara, dissertation, University of Tokyo, 1988.
[20]M. Ichimura *et al.*, Proceedings of the International Conference on Spin Observables of Nuclear Probes, 1988 (unpublished).
[21]R. D. Smith, Proceedings of the International Conference on Spin Observables of Nuclear Probes, 1988 (unpublished).
[22]U. Stroth *et al.*, Phys. Lett. **156B**, 291 (1985).
[23]H. Esbensen and G. F. Bertsch, Ann. Phys. (N.Y.) **157**, 255 (1984).
[24]S. Shlomo and G. F. Bertsch, Nucl. Phys. **A243**, 507 (1975).
[25]H. Toki and W. Weise, Phys. Rev. Lett. **42**, 1034 (1979); Z.

Phys. A **292**, 389 (1979).
[26]Y. Horikawa, F. Lenz, and N. C. Muhkopadhyay, Phys. Rev. C **22**, 1680 (1980); A. Dellafiore, F. Lenz, and F. A. Brieva, *ibid.* **31**, 1088 (1985); F. A. Brieva and A. Dellafiore, *ibid.* **36**, 899 (1987).
[27]T. Izumoto, Nucl. Phys. **A395**, 189 (1983).
[28]T. Izumoto, M. Ichimura, C. M. Ko, and P. J. Siemens, Phys. Lett. **112B**, 315 (1982).
[29]F. Osterfeld, D. Cha, and J. Speth, Phys. Rev. C **31**, 372 (1985).
[30]W. M. Alberico, A. De Pace, and A. Molinari, Phys. Rev. C **31**, 2007 (1985).
[31]T. Izumoto and A. Mori, Phys. Lett. **82B**, 163 (1979).
[32]A. L. Fetter and J. D. Walecka, *Quantum Theory of Many Particle System* (McGraw-Hill, New York, 1971).
[33]A. Picklesimer *et al.*, Phys. Rev C **30**, 1861 (1984).
[34]G. R. Satchler, *Direct Nuclear Reactions* (Clarendon, Oxford, 1983).
[35]D. V. Bugg and C. Wilkin, Phys. Lett. **152B**, 37 (1985); Nucl. Phys. **A467**, 575 (1987).
[36]A. Bohr and B. Mottelson, *Nuclear Structure* (Benjamin, New York, 1975), Vol. 1.
[37]T. Cheon, K. Shimizu, and A. Arima, Phys. Lett. **138B**, 345 (1984).
[38]N. V. Giai, P. F. Bortignon, F. Zardi, and R. A. Broglia, Phys. Lett. B **199**, 155 (1987).
[39]B. C. Clark *et al.*, Phys. Lett. **122B**, 211 (1983).
[40]K. Shimizu, M. Ichimura, and A. Arima, Nucl. Phys. **A226**, 282 (1974); G. F. Bertsch and I. Hamamoto, Phys. Rev. C **26**, 1323 (1982); S. Drożdż, F. Osterfeld, J. Speth, and J. Wambach, Phys. Lett. B **185**, 287 (1987); K. Takayanagi, K. Shimizu, and A. Arima, Nucl. Phys. **A477**, 205 (1988); **A477**, 313 (1988); R. D. Smith and J. Wambach, Phys. Rev. C **38**, 100 (1988).
[41]Nguyen van Giai and Pham van Thieu, Phys. Lett. **126B**, 421 (1983); C. Mahaux and R. Sartor, Nucl. Phys. **A481**, 381 (1988), and references therein.
[42]G. F. Bertsch and S. F. Tsai, Phys. Rep. **18**, 125 (1975); N. Auerbach and A. Klein, Nucl. Phys. **A452**, 398 (1986).
[43]X. Q. Zhu, N. Mobed, and S. S. M. Wong, Nucl. Phys. **A466**, 623 (1987).
[44]G. Orlandini, M. Traini, and M. Ericson, Phys. Lett. B **179**, 201 (1986).